Synchronous Vibration Control of MSCSG Based on High-Precision Closed-Loop Synchronous Rotating Frame Transformation

Wenjing Han, Yuanwen Cai, Wenting Han, Chunmiao Yu, Yuan Ren, *Member, IEEE*, Weijie Wang, and Zengyuan Yin

***Abstract*—Due to rotor mass imbalance, magnetic suspension control sensitive gyroscope (MSCSG) has synchronous vibration. In order to reduce the influence of the above unbalance vibration on the performance of MSCSG and the measurement accuracy of angular velocity, a method to suppress the imbalance vibration based on the high-precision closed-loop synchronous rotating frame transformation method is proposed. First, the unbalance vibration torque dynamics model of MSCSG with mass unbalance was established, and the influence of unbalance vibration on the measurement accuracy of attitude angular velocity was analyzed. Then, a high-precision closed loop synchronous rotating frame transformation (HCSRF) controller is designed. A high-precision closed loop detection method including PI controller and low pass filter is used to improve the detection accuracy of synchronous signal. A HCSRF controller is used to suppress synchronous disturbance current of two channels simultaneously. Finally, aiming at the dual-input and output and strong coupling characteristics of tilt channel, the equivalent conversion method is used to analyze the stability of system. Simulation and experimental results show that the proposed method can effectively suppress synchronous disturbance current and vibration torque, and reduce the influence of mass unbalance on the MSCSG performance and angular velocity measurement accuracy.**

***Index Terms*—Magnetic bearing, magnetically suspended control and sensitive gyroscope (MSCSG), synchronous rotating frame transformation, unbalance vibration.**

I. Introduction

With the development of space missions, magnetic bearings with advantages of high speed, active control, no friction and long life have been widely used in inertial actuators of spacecraft, such as magnetically suspended flywheels and magnetically suspended control moment gyro. By magnetically suspended technology, the rotor is suspended without contact [1], [2], [3], [4].

Although magnetically suspended inertial actuators has the above advantages, when the rotor rotates at high speed, the uneven mass distribution of the material and installation errors will lead to the existence of rotor mass imbalance. The mass unbalance of rotor is divided into static unbalance and dynamic unbalance [5], [6], [7], which will produce synchronous vibration force and synchronous vibration torque [8], [9].The above vibration force and torque are transferred to the spacecraft platform, which will seriously affect the pointing accuracy and ultra agile maneuvering performance of the spacecraft. Therefore, it is necessary to suppress the unbalanced vibration in the magnetically suspended rotor.

Physical vibration isolation devices are used to suppress vibration of spacecraft. Although it is possible to convert small high-frequency vibration to large low-frequency vibration, in essence, the vibration is not eliminated, but only blocking the transmission of it. In addition, the isolation will bring additional hardware burden to the spacecraft attitude control system and each vibration isolation can not completely suppress the vibration of all frequency bands. In order to solve above problems, the active vibration control technology is used to suppress microvibration by taking advantage of the active control of the rotor. Active vibration control technology only needs software loading, and the algorithm is more universal, only considering the magnetically suspended rotor control system itself, which can take into account the suppression effect of all frequency bands.

Notch filter is one of the active vibration control methods. The conventional notch filter has the advantages of simple structure and easy implementation, but it will affect the stability of the magnetically suspended rotor system. In order to ensure the stability of the rotor in full speed range, it is improved by introducing the phase shift angle, changing the connection mode, adding switching point, and so on. In [10], a parallel mode phase-shift notch filter is proposed, and compared with the series mode, it can suppress synchronous vibration better. In [11], a two-stage notch filter is proposed to suppress synchronous vibration of magnetically suspended rotor system with significant gyroscopic effect. The solution of the two-stage switching point

Manuscript received 20 September 2023; revised 31 March 2024 and 16 May 2024; accepted 28 June 2024. Date of publication 2 July 2024; date of current version 28 January 2025. This work was supported by the National Natural Science Foundation of China under Grant 52075545. Recommended for publication by Associate Editor R. Kennel. *(Corresponding authors: Yuanwen Cai; Chunmiao Yu.)*

Wenjing Han, Yuanwen Cai, Wenting Han, Chunmiao Yu, Yuan Ren, and Weijie Wang are with the Space Engineering University, Beijing 101416, China (e-mail: hwj_pll@163.com; 2534667068@qq.com; hwtcucurbit@163.com; yuchunmiao@buaa.edu.cn; renaun_823@aliyun.com; wangwjie@126.com).

Zengyuan Yin is with the Astronaut Center of China, Beijing 100094, China (e-mail: Freeyzy1@163.com).

Color versions of one or more figures in this article are available at https://doi.org/10.1109/TPEL.2024.3421965.

Digital Object Identifier 10.1109/TPEL.2024.3421965

is derived to distinguish low speed and high speed to ensure the stability of the system in the full speed range. Peng et al. [12], aiming at the problem of significant gyroscopic effect and severe coupling dynamics in magnetically suspended flywheel, proposed a novel cross-feedback notch filter and analyze the stability of the coupled MIMO system based on complex-coefficient stability criterion. In [13], an adaptive notch filter is proposed, which can adjust the notch depth and center frequency. However, the above improved notch filter still have some problems, such as affecting the stability of the magnetically suspended rotor system and causing greater vibration when the polarity switch or two-stage switch is switched.

In addition to synchronous vibration suppression methods based on notch filter, there are also methods of least-mean-squares (LMS) algorithm, repetitive control, resonant controller [14], [15], [16], adaptive multifrequency estimation (AMFE) algorithm. LMS algorithm is a discrete adaptive notch filter in essence [17], [18]. It has simple principle and strong robustness, but it requires a lot of computation and convergence rate is slow. Cui et al. [19] proposed a method based on frequency-domain adaptive LMS. By improving the updating strategy of the step size and convergence rate of the conventional LMS algorithm, the harmonic vibration force of magnetically suspended rotor system is effectively suppressed. Repetitive control can suppress periodic disturbance signals with known period, unknown amplitude and multifrequency components, but when the frequency changes, there are problems such as slow response speed and poor robustness [20], [21], [22]. Cui et al. [23] proposed an odd-harmonic fractional repetitive controller, which can effectively suppress odd-disturbance current with pertinence at low rotation speed with less computational burden and faster convergence rate. The above methods for synchronous vibration suppression all require the speed of the rotational rotor. When the Hall speed sensor has a large measurement error or fails, it is necessary to estimate the actual speed signal of the rotor. AMFE algorithm can not only suppress synchronous vibration, but also estimate the actual speed of rotor with reasonable algorithm design [24], [25], [26], [27]. However, its principle is complicated and the influence of controller on the stability of the two channels should be considered at the same time.

In addition to the above methods to suppress synchronous and harmonic vibration in magnetically suspended rotor system, the synchronous rotating frame (SRF) transformation is often used in this filed because of its simple structure, easy implementation, few adjustable parameters, and less computational burden. Zheng et al. [28] first restrained synchronous vibration of active magnetic bearing system by SRF method. Considering the serious gyroscope effect in magnetically suspended flywheel system, an improved SRF method is proposed in [29], which can effectively suppress synchronous vibration torque and ensure the stability of the system through phase compensation. Peng and Zhou [30] proposed a direct vibration force suppression based on an improved SRF method, which takes the synchronous vibration force as the input signal of SRF controller instead of the displacement signal to suppress synchronous vibration force directly. In [31], a high-precision synchronous signal detection method based on SRF is proposed aiming at the low accuracy of open-loop detection method caused by the phase lag of the low-pass filter (LPF) in the traditional SRF method, which improves the suppression affect. Cui et al. [32] proposed a multisynchronous rotating frame transformation method, which suppress vibration force by one controller simultaneously, saving computing resources and having faster response speed. However, due to the introduction of a LPF and the open-loop detection method, the conventional SRF method has serious phase lag and low suppression accuracy.

Magnetically suspended control and sensitive gyroscope (MSCSG) is a new type of spacecraft inertial device. It realizes attitude control and angular velocity measurement by high-speed rotating magnetically suspended rotor [33], [34], [35]. In order to realize the above functions, according to the control principle of MSCSG, the corresponding control system is designed, which mainly includes magnetic bearing, PID controller, power amplifier, and displacement sensor. There are two power amplifier boards in the control system and we choose the switch power amplifier, which is divided into two parts: 1) translational drive and 2) deflection drive.

According to the above simulation control model, the MSCSG hardware experiment system was established. The experimental system mainly includes MSCSG principle prototype, control circuit, oscilloscope, power supply, debugging computer, and so on. The power supply is used to supply power to other circuit board. The external power supply will provide 42 V stable voltage into the power supply board. And it will supply different voltage for other boards after the filter and dc–dc module. The control circuit is the core part of the MSCSG hardware system, which completes acquisition and conditioning of analog signal, processing signal, and power amplifier control output, respectively [36]. However, due to the rotor mass unbalance, the synchronous vibration torque will be generated when the rotor rotates at high speed, resulting in the disturbance current with the same frequency as the rotor speed in the rotor tilt control, which directly affects the accuracy of torque output and angular velocity measurement. Therefore, effective suppression of disturbance current caused by rotor unbalance vibration is the key to improve the attitude angular velocity measurement accuracy of MSCSG.

In order to reduce the influence of disturbance current on the attitude angular velocity measurement accuracy of MSCSG, after comparing the pros and cons of the above active vibration control methods in Table I, a novel synchronous vibration suppression method based on high-precision closed-loop synchronous rotating frame transformation (HCSRF) is proposed. The method has the following advantages.

1) It suppresses synchronous disturbance current of two tilt channels simultaneously by only one HCSRF controller, resulting in its simple structure, easy implementation, and low computational complexity.
2) In order to solve the problems of low suppression accuracy in open-loop detection link and serious phase lag in high frequency band of traditional SRF method, the PI controller and LPF are connected in parallel to form a closed-loop synchronous signal detection method, which

TABLE I
PROS AND CONS OF THE ACTIVE VIBRATION CONTROL METHODS

Method	Pros	Cons
Notch filter	Simple structure and easy implementation	Affect the stability
RC	Easy for discrete implementation	Slow response speed and poor robustness
RSC	Compensate for periodic signals	Not suitable for system with real-time frequency change
LMS	Simple principle and strong robustness	Lot of computation and slow convergence rate
AFE	Estimate the rotor speed	Complicated principle and large calculation
SRF	Few adjustable parameters and less computational burden	Phase lag and low detection accuracy

has higher detection accuracy and better suppression effect for synchronous vibration signal.

3) By adjusting the phase compensation factor, the stability of the system in the full speed range is guaranteed. In order to analyze the stability of tilt system, we take the MIMO cross-coupled system as SISO system equivalently in use of the orthogonality of MSCSG double-channel tilt angle.

Finally, the synchronous disturbance current and vibration torque caused by the rotor mass imbalance are suppressed, so its influence on the performance of MSCSG is reduced.

The rest of this article is organized as follows. In Section II, we introduce the unbalance vibration torque dynamics model of MSCSG with mass unbalance, and its influence on the measurement accuracy of attitude angular velocity. In Section III, we propose a synchronous vibration suppression method based on HCSRF and analyze its suppression effect on synchronous disturbance current and the influence on measurement accuracy of attitude angular velocity, and the stability of system is analyzed. The correctness of the proposed method is verified by simulation and experiments in Section IV. Finally, Section V concludes this article.

II. ANALYSIS OF THE INFLUENCE OF MASS IMBALANCE ON THE PERFORMANCE OF MSCSG

A. Structure of MSCSG

MSCSG is mainly composed of gyro room, radial magnetic bearing, axial magnetic bearing, Lorentz force magnetic bearing (LFMB), rotor system, drive motor, displacement sensor, and so on. As shown in Fig. 1, the radial magnetic bearing controls the radial two-degree-of-freedom (2-DOF) suspension and axial magnetic bearing controls the axial suspension with one DOF. LFMB mainly controls the 2-DOF tilt of the rotor and the high-speed rotation is controlled by a drive motor. According to Ampere's law, there is a linear relationship between the force generated by the LFMB and the coil current, which can measure the 2-DOF tilt of the rotor.

As shown in Fig. 2, LFMB is composed of stator system and rotor system. The stator consists of a stator skeleton and coils. The rotor mainly consists of inner permanent magnets and outer permanent magnets. In order to close the magnetic circuit, the

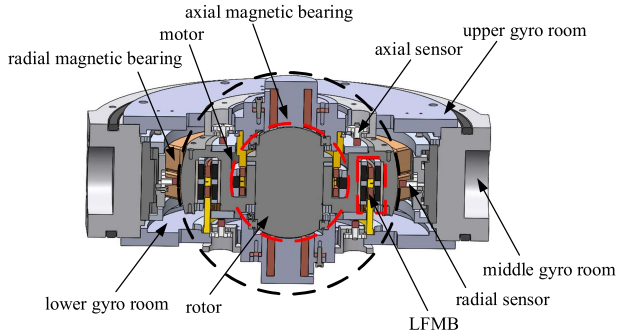

Fig. 1. MSCSG section diagram.

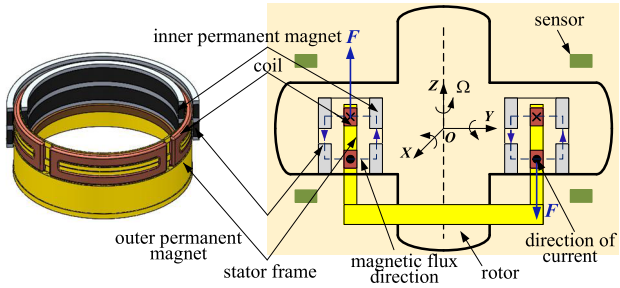

Fig. 2. Structure diagram of LFMB.

inner permanent magnets and the outer permanent magnets are divided into upper and lower layers, which have same magnetizing direction in the same layer, while the magnetizing direction of them in the upper and lower layers is opposite. Four coils are used in series in pairs and wound around the stator skeleton.

B. Modeling of Unbalance Vibration Torque With Mass Unbalance

According to the generation principle of MSCSG tilt torque [37], [38], the electromagnetic torque generated by LFMB can be expressed as

$$\begin{cases} M_\alpha = 4NBI_y{L_r}^2\varphi \\ M_\beta = 4NBI_x{L_r}^2\varphi \end{cases} \tag{1}$$

where M_α and M_β are the 2-DOF control torques output by LFMB, N represents the number of turns of the coil, I_x and I_y represent the control current, B represents the magnetic field strength of LFMB, L_r represents the radius of stator skeleton, and φ represents the central angle corresponding to the coil.

And according to the technical equation of the gyro, the tilt dynamic equation of MSCSG is

$$\begin{cases} M_x = J_x\ddot{\alpha} + J_z\Omega\dot{\beta} \\ M_y = J_y\ddot{\beta} - J_z\Omega\dot{\alpha} \end{cases} \tag{2}$$

where J_x, J_y, and J_z are the moments of inertia of the rotor about each axis, $\dot{\alpha}$ and $\dot{\beta}$ are the rotational angular velocities of the rotor about the x-axis and y-axis, respectively, and Ω is the rotor speed. Because the torque of rotor tilt is only controlled by

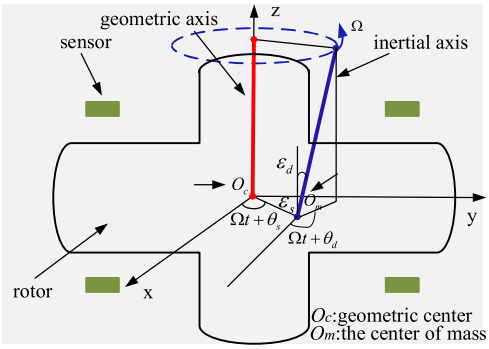

Fig. 3. Rotor mass unbalance of MSCSG.

LFMB, so we can get

$$\begin{cases} M_x = M_\alpha \\ M_y = M_\beta. \end{cases} \tag{3}$$

From (1), (2), and (3), we can obtain: the model of rotor tilt control model

$$\begin{cases} J_x\ddot{\alpha} + J_z\Omega\dot{\beta} = 4NBI_y{L_r}^2\varphi \\ J_y\ddot{\beta} - J_z\Omega\dot{\alpha} = 4NBI_x{L_r}^2\varphi \end{cases}. \tag{4}$$

The essence of the rotor dynamic unbalance is that the inertial axis is inconsistent with the geometric axis, so there is an angle. And the sensor detects the tilt angle, which is symmetry of the geometric axis. But the tilt angle will fluctuate as the rotor speed when the rotor rotates around the rotation axis. As shown in Fig. 3, the tilt angle detected by sensor can be expressed

$$\begin{cases} \alpha_r = \alpha + \varepsilon_d\cos(\Omega t + \theta_d) \\ \beta_r = \beta + \varepsilon_d\sin(\Omega t + \theta_d) \end{cases} \tag{5}$$

where α and β represent the rotor tilt angle in ideal conditions; α_r and β_r represent the actual tilt angle affected by mass unbalance; ε_d and θ_d represent, respectively, the eccentricity and initial phase between the inertial axis and the geometric axis.

The fluctuation of tilt angle will generate the synchronous disturbance current through the controller and power amplifier, and generate synchronous vibration torque through the torque coefficient. Where the synchronous disturbance current I_{xs} and I_{ys} can be expressed as

$$\begin{cases} I_{\mathrm{xs}} = \chi_x\cos(\Omega t + \theta_d) \\ I_{ys} = \chi_y\sin(\Omega t + \theta_d) \end{cases} \tag{6}$$

where χ_x and χ_y represent the coefficient of synchronous harmonic current, which is related to the rotor speed and increases when the speed increases.

Substituting (5) into (2),we can get

$$\begin{cases} M_x + (J_x - J_z)\varepsilon_d\Omega^2\cos(\Omega t + \theta_d) = J_x\ddot{\alpha} + J_z\Omega\dot{\beta} \\ M_y + (J_y - J_z)\varepsilon_d\Omega^2\sin(\Omega t + \theta_d) = J_y\ddot{\beta} - J_z\Omega\dot{\alpha} \end{cases}. \tag{7}$$

Let

$$\begin{cases} M_{d\alpha} = (J_x - J_z)\varepsilon_d\Omega^2\cos(\Omega t + \theta_d) \\ M_{d\beta} = (J_y - J_z)\varepsilon_d\Omega^2\sin(\Omega t + \theta_d) \end{cases}. \tag{8}$$

These are the synchronous vibration torques generated by the rotor dynamic unbalance.

C. Influence of Rotor Mass Unbalance on Angular Velocity Measurement Accuracy

In the inertial coordinate system, the attitude angular velocity and angular acceleration of the spacecraft are, respectively, $\boldsymbol{\omega_s} = [\omega_x\omega_y\omega_z]$, $\dot{\boldsymbol{\omega}}_\mathbf{s} = [\dot{\omega}_x\dot{\omega}_y\dot{\omega}_z]$. The tilt angular velocity and angular acceleration of the magnetically suspended rotor are, respectively, $\boldsymbol{\omega_r} = [\dot{\alpha}\dot{\beta}\dot{\Omega}]$, $\dot{\boldsymbol{\omega}}_\boldsymbol{r} = [\ddot{\alpha}\ddot{\beta}\ddot{\Omega}]$.

It can be seen from (4) that the tilt dynamic equation of MSCSG in the inertial coordinate system is

$$\begin{cases} J_x(\ddot{\alpha} + \dot{\omega}_x) + J_z\Omega(\dot{\beta} + \omega_y) = 4NBI_y{L_r}^2\varphi \\ J_y(\ddot{\beta} + \dot{\omega}_y) - J_z\Omega(\dot{\alpha} + \omega_x) = 4NBI_x{L_r}^2\varphi \end{cases}. \tag{9}$$

Assuming that the attitude angular acceleration of the spacecraft is very small, $\ddot{\alpha} \gg \dot{\omega}_x$,$\ddot{\beta} \gg \dot{\omega}_y$, (9) can be simplified as

$$\begin{cases} J_x\ddot{\alpha} + J_z\Omega(\dot{\beta} + \omega_y) = 4NBI_y{L_r}^2\varphi \\ J_y\ddot{\beta} - J_z\Omega(\dot{\alpha} + \omega_x) = 4NBI_x{L_r}^2\varphi \end{cases}. \tag{10}$$

From (10), attitude angular velocity measurement principle of MSCSG can be expressed

$$\begin{cases} \omega_x = -\frac{K}{h}i_x - \dot{\alpha} + \frac{J_y}{h}\ddot{\beta} \\ \omega_y = \frac{K}{h}i_y - \dot{\beta} - \frac{J_x}{h}\ddot{\alpha} \end{cases} \tag{11}$$

where $K = 4NBI_y{L_r}^2\varphi$ is the torque coefficient of MSCSG and h is the angular momentum of the rotor. From (11), it can be seen that the attitude angular velocity of the spacecraft can be measured when the control current of LFMB, tilt angular velocity and acceleration of the magnetically suspended rotor are known.

Considering the rotor mass imbalance, the drift error model of MSCSG angular velocity measurement is established

$$\begin{cases} \omega_{dx} = D_0(x) + D_1a_x + D_2a_xa_z + \varepsilon_x \\ \omega_{dy} = D_0(y) + D_1a_y + D_2a_ya_z + \varepsilon_y \end{cases} \tag{12}$$

where $D_0(x)$ is the constant interference torque coefficient caused by dynamic unbalance, and D_1 and D_2 are the drift error coefficients proportional to the acceleration and quadratic acceleration, respectively. a_x, a_y, and a_z are the accelerations of the X-axis, Y-axis, and Z-axis, respectively; $\varepsilon_x$and $\varepsilon_y$are random drift errors.

From (6), (11), and (12), the constant interference torque coefficient caused by mass dynamic unbalance is

$$\begin{cases} D_0(x) = -\frac{K}{h}\chi_x\cos(\Omega t+\theta_d) + \varepsilon_d\Omega\sin(\Omega t+\theta_d)\cdot(1-\frac{J_y}{h}\Omega) \\ D_0(y) = \frac{K}{h}\chi_y\sin(\Omega t+\theta_d) - \varepsilon_d\Omega\cos(\Omega t+\theta_d)\cdot(1-\frac{J_x}{h}\Omega) \end{cases}. \tag{13}$$

As can be seen from (13), the synchronous disturbance current and fluctuation of rotor tilt angle caused by rotor mass dynamic unbalance will affect the accuracy of attitude angular velocity measurement of MSCSG.

Therefore, we need compensate the rotor mass unbalance through active vibration control to eliminate synchronous displacement signal detected in the displacement sensor. The method of active vibration control is needed to carry out unbalance compensation to eliminate synchronous displacement

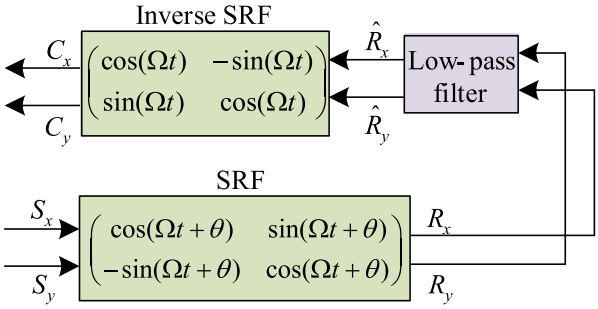

Fig. 4. Schematic diagram of SRF with open-loop method torque.

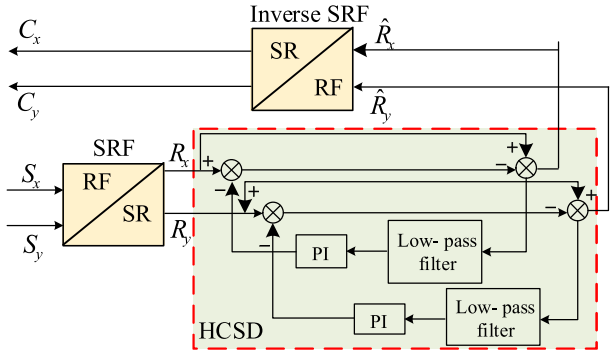

Fig. 5. Schematic diagram of HCSRF method.

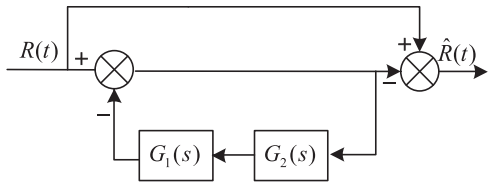

Fig. 6. Simplified block diagram of the HCSD method.

signal detected by the displacement sensor and suppress the fluctuation of rotor tilt angle, and finally eliminate the synchronous disturbance current and vibration.

III. Design and Analysis of HCSRF Transformation Algorithm

A. Principle and Structure of SRF

According to the principle of rotor mass unbalance, the center of mass of the rotor does not coincide with the geometric center. When the rotor is rotating at high speed, the frequency of unbalance vibration is the same as the rotor speed. Therefore, the output signal of the displacement sensor contains components of the same frequency as the rotor speed. Assume that the dual-channel orthogonal ac signals output by the displacement sensor are S_x and S_y, and the dc signals through the synchronous rotating frame are R_x and R_y.

Fig. 4 is the general structure of the open-loop SRF transformation. Define S_x-O_m-S_y as the fixed sensor coordinate system, R_x-O_m-R_y as the synchronous rotating coordinate system, O_m is the center of mass of the rotor, and O_c is the rotor geometric center. Let (s_x,s_y) and (r_x,r_y) denote the coordinate of O_c in the fixed sensor coordinate system and the synchronous rotating frame. When the rotor rotates at a constant speed Ω, the relationship of SRF can be expressed as

$$\begin{pmatrix} R_x \\ R_y \end{pmatrix} = \begin{pmatrix} \cos(\Omega t+\theta) & \sin(\Omega t+\theta) \\ -\sin(\Omega t+\theta) & \cos(\Omega t+\theta) \end{pmatrix} \begin{pmatrix} S_x \\ S_y \end{pmatrix} \tag{14}$$

where θ is the phase compensation factor to ensure the stability of the system in the full speed range.

After SRF, R_x and R_y contain both synchronous signals and high-frequency noise. Therefore, a LPF is needed for filtering. Here, we adopt a first-order LPF:

$$G_f(s) = \frac{1}{\tau s+1} \tag{15}$$

where τ is the time constant of LPF. The filtered dc signal only contains synchronous vibration signals and the high-frequency noise is filtered out.

Finally, from (15), the dc signal after LPF will be ac signal through the inverse SRF transformation

$$\begin{pmatrix} C_x \\ C_y \end{pmatrix} = \begin{pmatrix} \cos(\Omega t) & -\sin(\Omega t) \\ \sin(\Omega t) & \cos(\Omega t) \end{pmatrix} \begin{pmatrix} \hat{R}_x \\ \hat{R}_y \end{pmatrix} \tag{16}$$

where $\hat{R}_x$ and $\hat{R}_y$ are dc signals after LPF, C_x and C_y are vibration signals of the same frequency as the rotational speed, which can be reversed and compensated into the original system to eliminate the synchronous vibration signals of the displacement signal caused by the rotor mass unbalance.

B. Principle and Structure of HCSD Method

According to the principle of SRF, in order to improve the suppression effect, it is necessary to accurately detect the synchronous components of dc signal after SRF transformation. The traditional SRF algorithm uses the open-loop detection method. Although the first-order LPF has simple structure and low computational complexity, the detection accuracy is lower and there is phase lag in the high frequency band, which seriously affects the compensation effect of synchronous dc signal obtained after the inverse SRF transformation. In order to solve above problems, HCSRF based on high-precision closed-loop synchronous signal detection (HCSD) method is proposed, which can suppress synchronous vibration signals precisely, as shown in Fig. 5.

Fig. 5 is a schematic diagram of HCSRF based on HCSD method. Some part of the dc signal converted by SRF transformation directly enters the output of HCSD system, and the other part is negatively fed back from the output to the input through connecting in series with PI controller and LPF, forming the HCSD system. Fig. 6 is the simplified block diagram of HCSD method of synchronous signal. Where G_1 is the PI controller and G_2 is LPF, which can be expressed as

$$\begin{cases} G_1(s) = k_p + \frac{k_i}{s} \\ G_2(s) = \frac{1}{\tau s+1}. \end{cases} \tag{17}$$

Therefore, the closed-loop transfer function of HCSD is

$$G_{\mathrm{HCSD}}(s)=\frac{G_1G_2}{1+G_1G_2}=\frac{k_ps+k_i}{\tau s^2+(k_p+1)\,s+k_i}. \tag{18}$$

Equations (14) and (16) can be represented by using the exponential expression as

$$\begin{cases} R(t)=S(t)\cdot e^{-j(\Omega t+\theta)} \\ C(t)=\hat{R}(t)\cdot e^{j\Omega t} \end{cases}. \tag{19}$$

Applying Laplace transformation to (19) results in

$$\begin{cases} R(s)=S(s+j\Omega)\cdot e^{-j\theta} \\ C(s)=\hat{R}(s-j\Omega) \end{cases}. \tag{20}$$

As shown in Fig. 6, it can be obtained that

$$\hat{R}(s)=R(s)\cdot G_{\mathrm{HCSD}}(s). \tag{21}$$

Combining (20) and (21) yields

$$\begin{cases} \hat{R}(s)=S(s+j\Omega)\cdot e^{-j\theta}\cdot G_{HCSD}(s) \\ C(s)=S(s)\cdot e^{-j\theta}\cdot G_{HCSD}(s-j\Omega) \end{cases}. \tag{22}$$

As shown in Fig. 5, the open-loop transfer function of HCSRF transformation can be expressed as

$$\begin{aligned} G_{\mathrm{HCSRF}}(s)&=\frac{C(s)}{S(s)}=e^{-j\theta}\cdot G_{\mathrm{HCSD}}(s-j\Omega) \\ &=\frac{[k_p(s-j\Omega)+k_i]\cdot e^{-j\theta}}{\tau(s-j\Omega)^2+(k_p+1)\cdot(s-j\Omega)+k_i}. \end{aligned} \tag{23}$$

Thus, the closed-loop transfer function of HCSRF is

$$N_{\mathrm{HCSRF}}(s)=\frac{1}{1+kG_{\mathrm{HCSRF}}(s)}=\frac{\tau s^2+Ms-P}{\tau s^2+(M+N)s-P+Q} \tag{24}$$

where k is the closed-loop gain of HCSRF, and

$$\begin{cases} M=k_p+1-2\tau\cdot j\Omega \\ N=k\cdot k_p\cdot e^{-j\theta} \\ P=\tau\Omega^2+(k_p+1)\cdot j\Omega-k_i \\ Q=k(k_i-k_p\cdot j\Omega)\cdot e^{-j\theta}. \end{cases} \tag{25}$$

According to (24), the frequency characteristics of closed-loop transfer function of HCSRF is

$$N_{\mathrm{HCSRF}}(jw)\,|_{w=\Omega}=\frac{1}{1+\frac{kk_i\cdot e^{-j\theta}}{2\tau\Omega^2+k_i}}. \tag{26}$$

From (26), when$w\to\Omega$, there is$N_{\mathrm{HCSRF}}(jw)\to 0$. In addition, the notch depth is related to the gain k of HCSRF, the proportionality coefficient k_i of HCSD and the time constant τ of LPF.

C. Suppression of Synchronous Disturbance Current

According to the principle of rotor mass unbalance, the current in LFMB is composed of two parts: one part controls rotor stable suspension and tilt, and the other part is synchronous disturbance current, that is the current of LFMB

$$\begin{cases} I_{\mathrm{x}}=i_x+I_{xs} \\ I_y=i_y+I_{ys} \end{cases} \tag{27}$$

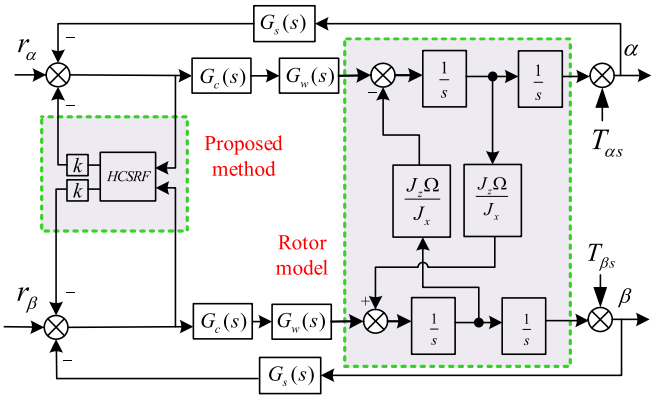

Fig. 7. Schematic diagram of synchronous vibration suppression method based on HCSRF.

where I_x and I_y are the rotor's tilt control current, i_x and i_y are the current controlling the rotor's stable suspension, and I_{xs} and I_{ys} are the synchronous disturbance current.

Fig. 7 is the control block diagram of MSCSG tilt channel based on HCSRF method. Where $G_c(s)$ is the transfer function of the controller, $G_w(s)$ is the transfer function of the power amplifier, $G_p(s)$ is the transfer function of the rotor radial control system, α and β are the tilt angle of α-axis and β-axis, and $T_{\alpha s}$ and $T_{\beta s}$ are the 2-DOF synchronous disturbance torque. It can be seen from that the rotor tilt control current through power amplifier can be expressed as

$$\begin{cases} I_{\mathrm{x}}=S_x\cdot G_s(s)\cdot G_c(s)\cdot G_w(s)\cdot\frac{1}{1+k\cdot G_{\mathrm{HCSRF}}(s)} \\ I_y=S_y\cdot G_s(s)\cdot G_c(s)\cdot G_w(s)\cdot\frac{1}{1+k\cdot G_{\mathrm{HCSRF}}(s)} \end{cases} \tag{28}$$

where

$$\begin{cases} S_{\mathrm{x}}=s_x+d_x \\ S_y=s_y+d_y \end{cases} \tag{29}$$

where s_x and s_y are the ideal sensor displacement signals of two tilt axis, d_x and d_y are the synchronous vibration signals caused by rotor mass imbalance, and S_x and S_y are the actual displacement signals of the displacement sensor.

By (27), (28), and (29), we can get

$$\begin{cases} I_{\mathrm{xs}}=d_x\cdot G_s(s)\cdot G_c(s)\cdot G_w(s)\cdot N_{\mathrm{HCSRF}}(s) \\ I_{ys}=d_y\cdot G_s(s)\cdot G_c(s)\cdot G_w(s)\cdot N_{\mathrm{HCSRF}}(s). \end{cases} \tag{30}$$

According to the analysis in the previous section, when$w\to\Omega$, there is $N_{\mathrm{HCSRF}}(jw)\to 0.$, so $I_{xs}\to 0$, $I_{ys}\to 0$. That is the synchronous disturbance component in the tilt control current, which is completely suppressed. From (41), there is

$$\begin{cases} I_{\mathrm{x}}\to i_x \\ I_y\to i_y \end{cases}. \tag{31}$$

From (31), we can know that the HCSRF method proposed in this article can effectively suppress the synchronous disturbance component in the tilt control current.

From (1), the generation principle of synchronous vibration torque can be expressed as

$$\begin{cases} T_{\alpha s}=I_{ys}4NBL_r^2\varphi \\ T_{\beta s}=I_{xs}4NBL_r^2\varphi \end{cases}. \tag{32}$$

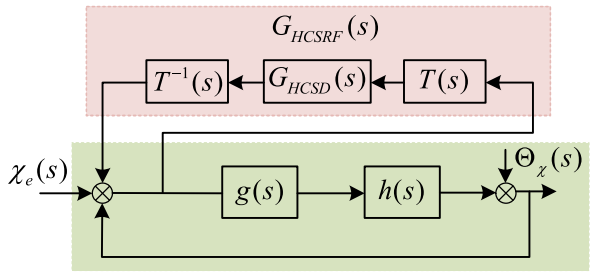

Fig. 8. Equivalent tilt control structure with HCSRF.

As can be seen from (32), when the synchronous disturbance current is suppressed, i.e., $I_{xs}\to 0$ and $I_{ys}\to 0$, there are $T_{\alpha s}\to 0$ and $T_{\beta s}\to 0$. So, when the synchronous disturbance current is effectively suppressed, the synchronous vibration torque is also completely suppressed. Combining (13) yields: $D_0(\mathrm{x})\to 0$, $D_0(\mathrm{y})\to 0$, i.e., constant interference torque coefficient caused by rotor mass dynamic unbalance tends to zero. From (12), we can know that it will effectively eliminate the influence of mass dynamic unbalance on the measurement accuracy of attitude angular velocity. So, the measurement accuracy of angular velocity is improved.

D. Stability Analysis

As can be seen from Fig. 7, the tilt control system of MSCSG can be expressed as

$$\begin{cases} J_x\ddot{\alpha}(t)+J_z\Omega\dot{\beta}(t)=G_cG_w(1-G_s)\alpha(t) \\ J_y\ddot{\beta}(t)-J_z\Omega\dot{\alpha}(t)=G_cG_w(1-G_s)\beta(t) \end{cases}. \tag{33}$$

From (33), we can know that the tilt control system of MSCSG is a MIMO cross-coupled system. In order to simplify the stability analysis of the system, it is necessary to transform it into a SISO system. Considering that the phase of rotor tilt angle β is 90°ahead of α. So, we define the complex variable $\chi=\alpha+j\beta$, where j is plural units 1. Combining with (32) and then applying Laplace transformation

$$J_rs^2\chi(s)-J_z\Omega s\chi(s)=G_c(s)G_w(s)[1-G_s(s)]\chi(s). \tag{34}$$

Therefore, the MIMO system is converted into a SISO system, and the characteristic equation of the tilt control system can be obtained from (33)

$$J_rs^2-J_z\Omega s-G_c(s)G_w(s)[1-G_s(s)]=0. \tag{35}$$

As can be seen from (35), the equivalent SISO system corresponds to a negative feedback control system. Where *g(s)* is equivalent control object transfer function, *h(s)* is equivalent control channel transfer function, respectively, expressed as

$$\begin{cases} g(s)=\frac{1}{J_rs^2-jJ_z\Omega s} \\ h(s)=G_c(s)G_w(s)[1-G_s(s)] \end{cases}. \tag{36}$$

Fig. 8 shows the control block diagram of equivalent SISO system about MSCSG tilt channel. Where T(s) is the SRF transformation and T^{-1}(s) is the inverse SRF transformation. The original sensitivity function of the system is defined as

$$S(s)=\frac{1}{1+g(s)h(s)}. \tag{37}$$

Let $\chi_e(s)$ is the input signal of equivalent SISO system, $\Theta_\chi(s)$ is the disturbance signal of equivalent SISO system. So, the transfer function from $\Theta_\chi(s)$ to $\chi_e(s)$is

$$\frac{\chi_e(s)}{\Theta_\chi(s)}=\frac{1}{1+g(s)h(s)+kG_{\mathrm{HCSRF}}(s)}. \tag{38}$$

Therefore, the characteristic equation of the reconstructed closed-loop system is

$$q(s)=1+g(s)h(s)+kG_{\mathrm{HCSRF}}(s). \tag{39}$$

By substituting (23) and (37) into (39), the closed-loop characteristic equation defined as the sensitivity function can be obtained

$$q(s)=L(s)+k[k_p(s-j\Omega)+k_i]e^{-j\theta}S(s) \tag{40}$$

where

$$L(s)=\tau(s-j\Omega)^2+(k_p+1)(s-j\Omega)+k_i. \tag{41}$$

Let $q(s)=0$, and if $k_i=0$, the root of the characteristic polynomial is $s=j\Omega$. Therefore, by substituting this condition into the characteristic equation and taking the derivative at $k_i=0$, we can get [39], [40]

$$\frac{\partial s}{\partial k_i}\Big|_{s=j\Omega,k_i=0}=-\frac{\partial q}{\partial k_i}\Big/\frac{\partial q}{\partial s}=-\left[k_p+\frac{1}{1+ke^{-j\theta}S(j\Omega)}\right]^{-1}. \tag{42}$$

In order to ensure the stability of system, the following conditions must be satisfied:

$$\frac{\pi}{2}<-\arg\left[k_p+\frac{1}{1+ke^{-j\theta}S(j\Omega)}\right]^{-1}<\frac{3\pi}{2}. \tag{43}$$

It can be seen from (43) that in order to satisfy the stability of the system within the full speed range, we should adjust the phase compensation factor θ when the rotor speed changes.

IV. Simulation and Experimental Verification

In order to verify the superiority and correctness of the proposed method, some simulations and experiments were carried out. Physical parameters and control parameters of the MSCSG system are shown in Tables II, III, and IV.

A. Simulation Analysis

First, the suppression effect of the proposed method at 83.3 Hz is simulated and analyzed. As shown in Fig. 9, the amplitude frequency response curve of HCSRF can be obtained from (23), and the suppression effect of the traditional SRF method and HCSRF is compared. When the rotor speed is 83.3 Hz, the time constant τ of first order LPF in SRF and HCSRF is set to 0.05. From the amplitude-frequency curve, the notch depth at 83.3 Hz is both at −35.3 dB, but HCSRF has narrower width at the center of notch, which can suppress the synchronous vibration signals with higher precision and less interference to signals in the surrounding frequency range. And the phase frequency curve

TABLE II
PHYSICAL PARAMETERS OF THE MSCSG SYSTEM

Symbol	Quantity	Value
J_x, J_y	Transverse moments of inertia	0.0097 kg·m^2
J_z	Polar moments of inertia	0.0166 kg·m^2
L_m	Inductance of coil	8.63 mH
R_m	resistance of coil	26.3 Ω
m	The weight of rotor	8.95 kg
K	Torque coefficient	2.1872 N·m/A
Ω	Rotor speed	523.12 rad/s

TABLE III
CONTROL PARAMETERS OF THE MSCSG SYSTEM (5000 R/MIN)

Symbol	Value	Symbol	Value
K_s	1	k_p	0.3
k_a	0.55	k_i	5
h_f	1.95	k	60
τ	0.05	θ	−20°

TABLE IV
CONTROL PARAMETERS OF THE MSCSG SYSTEM (4000 R/MIN)

Symbol	Value	Symbol	Value
K_s	1.2	k_p	0.2
k_a	0.52	k_i	8
h_f	1.91	k	75
τ	0.03	θ	−15°

shows that HCSRF method alleviates phase lag in the rotor speed range (0–83.3 Hz) compared with SRF method.

As can be seen from Fig. 5, two mutually orthogonal ac displacement signals are converted to dc signals through SRF frame, which consist of synchronous vibration signal and high-frequency noise. Then, the high-frequency noise is filtered out by HCSD system. In order to compare the filtering effect of LPF in traditional SRF method and HCSD in HCSRF method, Fig. 10 shows the output signal of dc signal through LPF and HCSD, respectively. As can be seen from Fig. 10, although the convergence speed of LPF is faster, it is only 0.002 s shorter than that of HCSD, which has little influence on the suppression effect of the unbalance vibration. In addition, the curve of LPF output signal is obviously rough, and the curve of HCSD output signal is smoother, i.e., the filtering effect of high-frequency noise is better, and the suppression effect of unbalanced vibration is better. Therefore, the proposed method uses HCSD instead of LPF.

In order to verify the adjustment effect of phase compensation factor θ on the system stability at full rotational speed (0–5000 r/min), the closed-loop root locus of the system with different θ is compared. Fig. 11 shows the root locus under three conditions as follows:

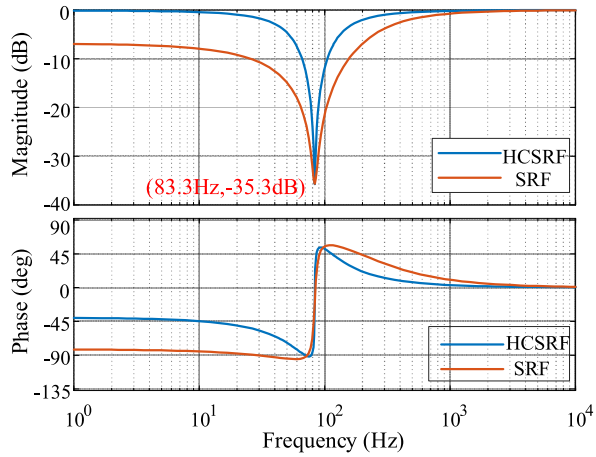

Fig. 9. Amplitude frequency response curve of the HCSRF method when rotor speed is 83.3 Hz ($\tau = 0.05$, k = 60, kp = 0.3, ki = 5).

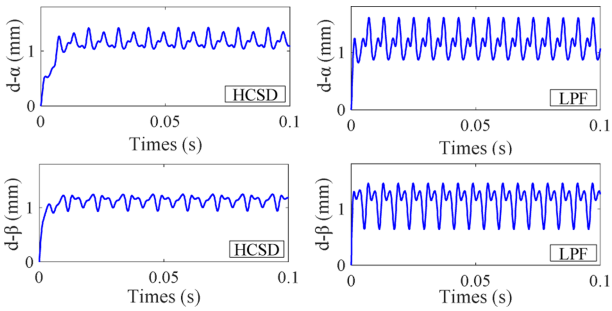

Fig. 10. Output signal of HCSD system and LPF of α channel and β channel.

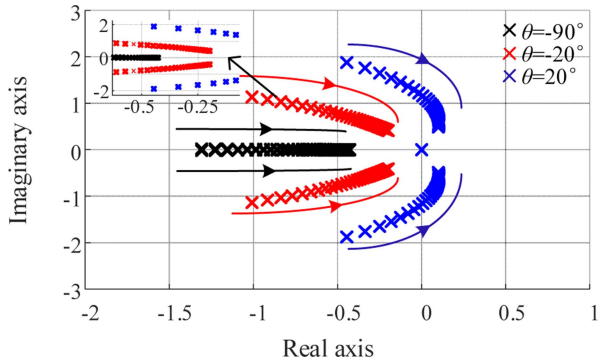

Fig. 11. Closed-loop root trajectory of the HCSRF when $\theta = -90°$, $\theta = -20°$, $\theta = 20°$ at full rotational speed (0–5000 r/min).

$\theta = -90°$, $\theta = -20°$, $\theta = 20°$. As can be seen from Fig. 11, when the rotor speed increases from 0 r/min to the rated speed of 5000 r/min, the damping of pole gradually decreases and the stability of the system is deteriorated. However, by adjusting θ, the stability of the system can be ensured. As θ increases from $-90°$ to 20°, the poles of the system move to the right gradually, and when $\theta = 20°$, some poles are distributed in the right half plane, so the system is unstable. When $\theta < 0°$, the poles move to the left with θ decreases and the damping of the system increases gradually, so the stability of the system is enhanced. However,

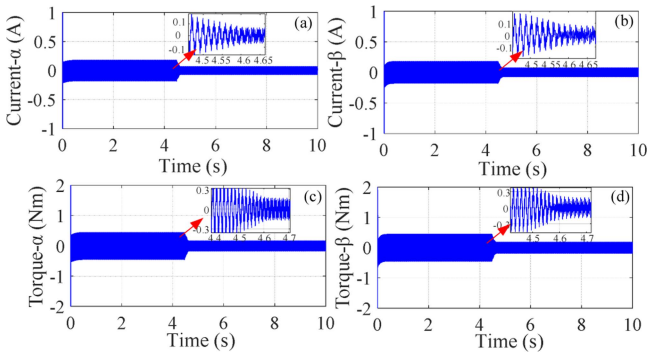

Fig. 12. Simulation results of current at a speed of 4000 r/min with the proposed method at t = 3 s. (a) Control current in α-axis. (b) Control current in β-axis. (c) Vibration torque in α-axis. (d) Vibration torque in β-axis.

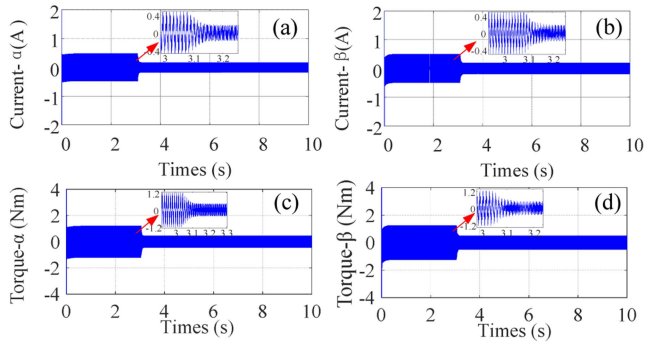

Fig. 13. Simulation results of current at a speed of 5000 r/min with the proposed method at t = 3 s. (a) Control current in α-axis. (b) Control current in β-axis. (c) Vibration torque in α-axis. (d) Vibration torque in β-axis.

in this case, the suppression effect on synchronous vibration signals decreases. In order to balance the contradiction between the stability of the system and the suppression effect, we choose $\theta = -20°$ as the suitable value.

Figs. 12 and 13 show the simulation results when the rotor speed is 4000 r/min and 5000 r/min, respectively. As can be seen from them, when the HCSRF controller proposed is added at $t =$ 3 s, the synchronous control current and torque are effectively suppressed. When the rotor speed is 4000 r/min, the control current of α channel decreases from 176.5 mA to 68.4 mA, the control current of β channel decreases from 177.7 mA to 71.9 mA, the torque of α channel decreases from 0.444 Nm to 0.171 Nm, and the torque of β channel decreases from 0.449 Nm to 0.176 Nm. When the rotor speed is 5000 r/min, the control current of α channel decreases from 477.8 mA to 174.6 mA, the control current of β channel decreases from 479.1 mA to 194.2 mA, the torque of α channel decreases from 1.144 Nm to 0.429 Nm, and the torque of β channel decreases from 1.244 Nm to 0.476 Nm.

In order to verify the superiority of HCSRF method in suppressing the synchronous vibration signals, the same simulation parameters are set when the rotor speed is 5000 r/min, and the suppression effect was compared with SRF method. Fig. 14 shows the FFT analysis of torque when the rotor speed is 5000 r/min in three cases: 1) without suppression; 2) with SRF method; 3) with HCSRF method. As shown in Fig. 14, compared with the traditional SRF method, HCSRF not only has better suppression effect on the synchronous vibration torque, but also has less interference on the third and fifth harmonic component. Using SRF and HCSRF method, the synchronous torque of α channel is reduced by 89.89% and 90.07%, respectively, and β channel is reduced by 87.01% and 87.55%, respectively.

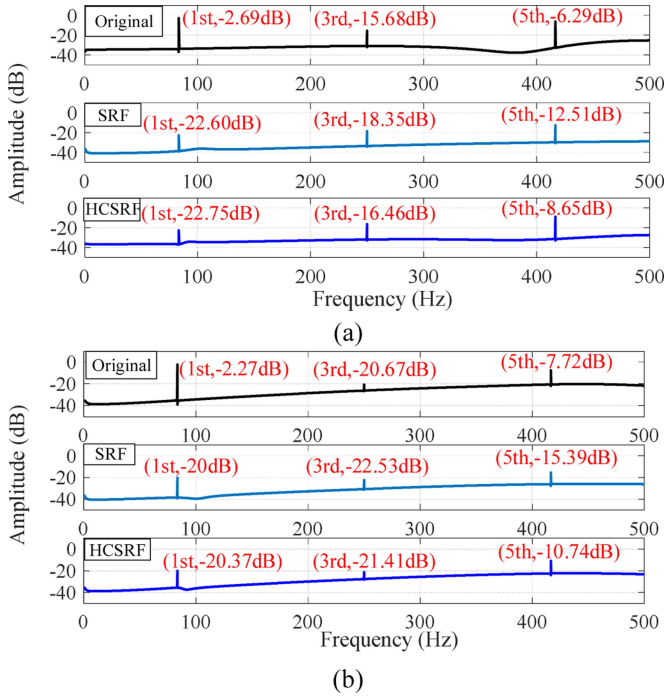

Fig. 14. FFT analysis of vibration torque at a speed of 5000 r/min without suppression, with SRF and HCSRF. (a) Vibration torque in α-axis. (b) Vibration torque in β-axis.

In order to verify the suppression effect of HCSRF method on synchronous vibration signals in the full speed range of 0–5000 r/min, the HCSRF method is applied during the rotor speed rises to the rated speed by simulation, and the results are shown in Fig. 15. As can be seen from Fig. 15, when the rated speed is reached, the synchronous vibration torque of α channel decreases from 0.76 dB to 0.07 dB, and β channel decreases from 0.79 dB to 0.1 dB.

B. Experimental Verification

In order to further illustrate the superiority and correctness of the proposed method, the suppression effect of synchronous disturbance current and vibration torque is verified by the MSCSG principle prototype system. The experimental system of MSCSG is shown in Fig. 16. The experimental system mainly includes a principle prototype of MSCSG, a control circuit, an oscilloscope, a power supply, and a debugging computer. The design of magnetic bearing control circuit is the focus of the whole system, which mainly includes three modules: 1) the conditioning module, 2) the signal processing module, and 3) the power amplifier module. The designed control circuit needs to process the signal, convert the sensor signal to A/D and

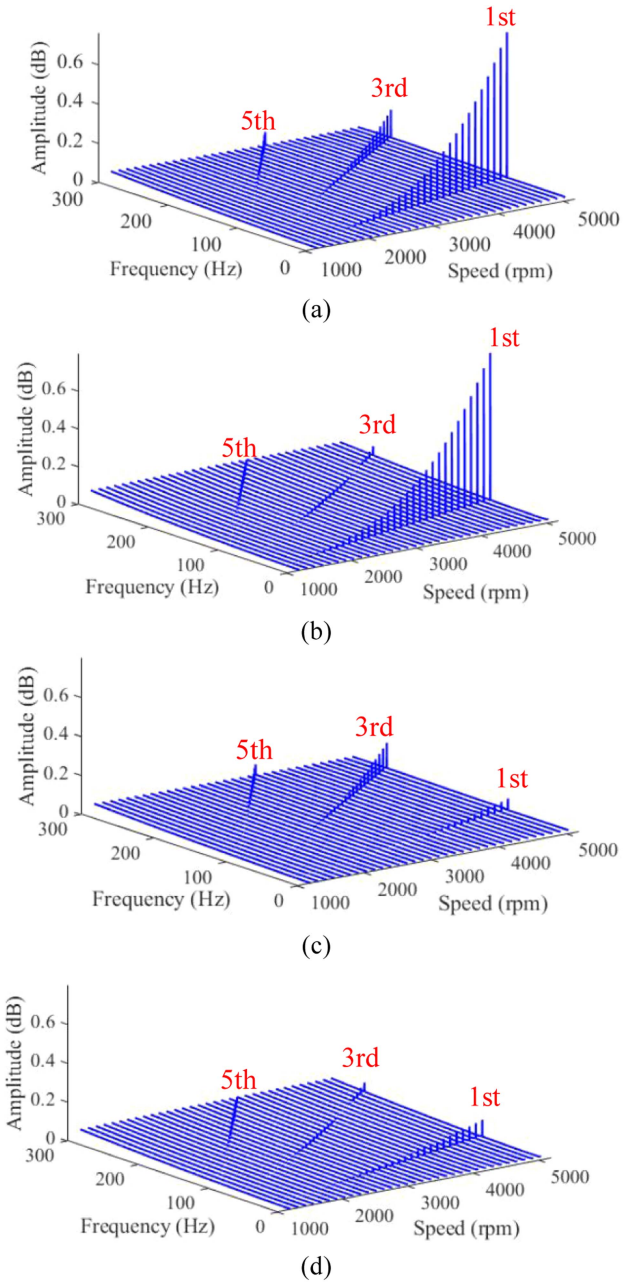

Fig. 15. Waterfall chart of vibration torque of MSCSG. (a) Without the proposed method in α-axis. (b) Without the proposed method in β-axis. (c) With HCSRF in α-axis. (d) With HCSRF in β-axis.

D/A, process the compiled control algorithm, and generate the corresponding control signal. The control signal is input into the winding of the magnetic bearing to complete the control function of the magnetic bearing.

The HCSRF method is used when the rotor speed is 4000 r/min and 5000 r/min, respectively. And they are compared with SRF method. The experimental results when the rotor speed is 4000 r/min are shown in Fig. 17. The blue curve is the time domain waveform of the control current, and the red curve is the spectrum analysis of it. As can be seen from Fig. 17, the unbalance vibration torque gradually increases with the increase

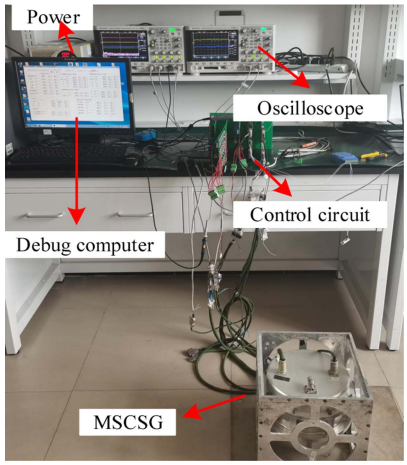

Fig. 16. Experimental system of MSCSG.

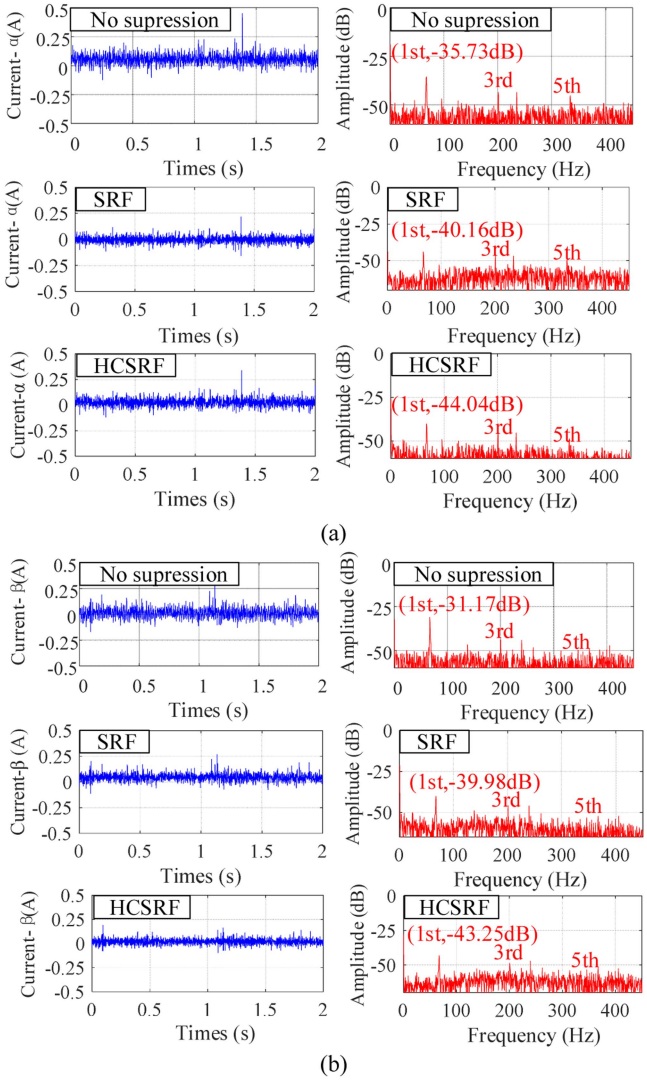

Fig. 17. Experimental results at a speed of 4000 r/min without the proposed method, with SRF and with HCSRF. (a) Control current in t in α-axis. (b) Control current in t in β-axis.

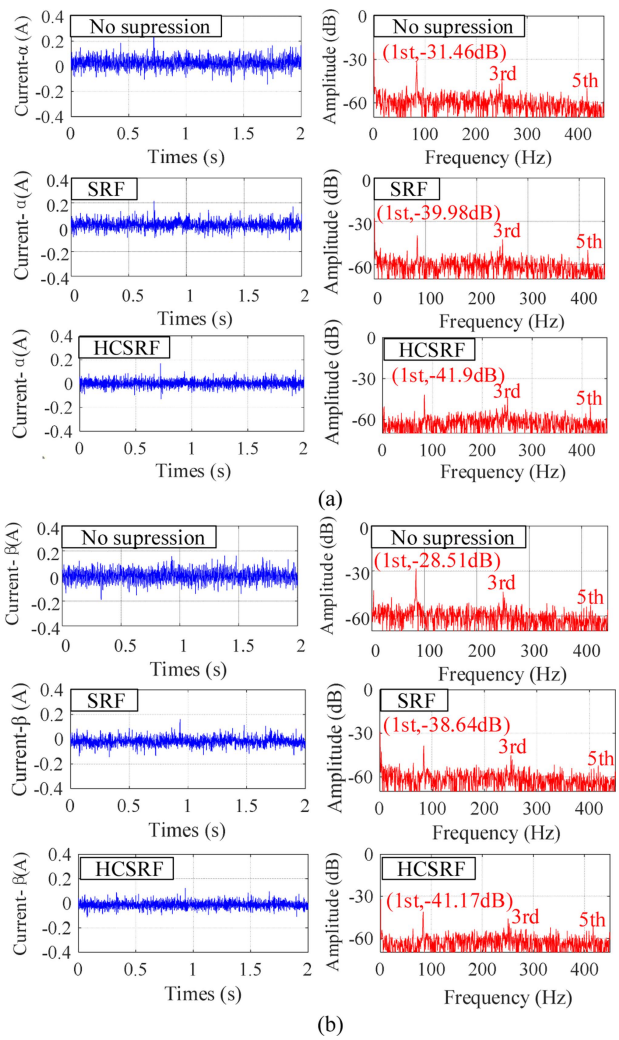

Fig. 18. Experimental results at a speed of 5000 r/min without the proposed method, with SRF and with HCSRF. (a) Control current in t in α-axis. (b) Control current in t in β-axis.

of rotor speed, and the synchronous vibration torque is the main interference component. Because the HCSRF method proposed in this article only suppress synchronous current and has no influence on the third and the fifth harmonic component current. According to the spectrum analysis, with HCSRF method, the synchronous disturbance current of α channel decreases by 87.64% from -35.73 dB to -44.04 dB and β channel decreases from -31.17 dB to -43.25 dB by 96.22%. And with SRF method, the synchronous disturbance current of α channel decreases by 68.93% and β channel decreases by 91.7%. So HCSRF method has better suppression effect.

The experimental results when the rotor speed is 5000 r/min are shown in Fig. 18. The amplitude of the synchronous current is larger than that at the speed of 4000 r/min, which conforms to the synchronous disturbance current of α channel decreases from -31.46 dB to -41.9 dB, reducing by 94.31%. And β channel decreases by 97.46% from -28.51 dB to -41.17 dB. And with SRF method, the synchronous disturbance current of α channel reduces by 90.9% and β channel reduces by 95.22%. The inhibition effect is not as good as HCSRF method.

According to the experimental results, the HCSRF method proposed in this article has obvious suppression effect on synchronous disturbance current, and has no influence on the third and fifth harmonic current. It can be seen from the relationship between torque and current that the proposed method also has obvious suppression effect on synchronous vibration torque.

V. Conclusion

The synchronous vibration torque caused by rotor mass unbalance will affect the accuracy of MSCSG's output torque and the measurement of attitude angular velocity. Although the traditional SRF method has simple structure and easy implement, it has some problems such as serious phase lag and low precision of synchronous vibration suppression. In order to improve the suppression effect of synchronous vibration torque, the HCSRF method is proposed, which only uses one controller to suppress the synchronous disturbance current of two tilt channels simultaneously in use of its orthogonality. The HCSD system including PI controller and LPF is adopted to improve the detection accuracy of synchronous signal and realize higher precision suppression effect. By adjusting the phase compensation factor, the stability of the system in the full speed range of the rotor is ensured. Simulation and experimental results demonstrate that the proposed method can effectively suppress synchronous disturbance current and vibration torque, which can reduce its influence on the attitude stability and ultra agile maneuvering performance of the spacecraft platform, and the attitude angular velocity measurement accuracy of MSCSG is improved.

References

[1] S. Zheng, B. Han, and L. Guo, "Composite hierarchical antidisturbance control for magnetic bearing system subject to multiple external disturbances," *IEEE Trans. Ind. Electron.*, vol. 61, no. 12, pp. 7004–7012, Dec. 2014, doi: 10.1109/TIE.2014.2316226.

[2] T. Matsuzaki, M. Takemoto, S. Ogasawara, S. Ota, K. Oi, and D. Mat-suhashi, "Novel structure of three-axis active-control-type magnetic bearing for reducing rotor iron loss," *IEEE Trans. Magn.*, vol. 52, no. 7, Jul. 2016, Art. no. 8105404, doi: 10.1109/TMAG.2016.2514604.

[3] X. Ye, Q. Le, and Z. Zhou, "A novel homopolar four degrees of freedom hybrid magnetic bearing," *IEEE Trans. Magn.*, vol. 56, no. 8, Aug. 2020, Art. no. 6703404, doi: 10.1109/TMAG.2020.3001935.

[4] B. Han, Y. Chen, S. Zheng, M. Li, and J. Xie, "Whirl mode suppression for AMB-rotor systems in control moment gyros considering significant gyroscopic effects," *IEEE Trans. Ind. Electron.*, vol. 68, no. 5, pp. 4249–4258, May 2021, doi: 10.1109/TIE.2020.2984463.

[5] J. D. Setiawan, R. Mukherjee, E. H. Maslen, and G. Song, "Adaptive compensation of sensor runout and mass unbalance in magnetic bearing systems," in *Proc. IEEE/ASME Int. Conf. Adv. Intell. Mechatronics*, 1999, pp. 800–805, doi: 10.1109/AIM.1999.803275.

[6] J. Fang, H. Zhang, and X. Xu, "Model development and disturbance current reduction in active magnetic bearing systems with rotor imbalance and sensor runout," *J. Vib. Control*, vol. 21, no. 13, pp. 2520–2535, 2015, doi: 10.1177/1077546313513624.

[7] C. Peng, S. Zheng, Z. Huang, and X. Zhou, "Complete synchronous vibration suppression for a variable-speed magnetically suspended flywheel using phase lead compensation," *IEEE Trans. Ind. Electron.*, vol. 65, no. 7, pp. 5837–5846, Jul. 2018, doi: 10.1109/TIE.2017.2782204.

[8] Q. Chen, G. Liu, and B. Han, "Suppression of imbalance vibration in AMB-rotor systems using adaptive frequency estimator," *IEEE Trans. Ind. Electron.*, vol. 62, no. 12, pp. 7696–7705, Dec. 2015, doi: 10.1109/TIE.2015.2455022.

[9] S. M. Darbandi, M. Behzad, H. Salarieh, and H. Mehdigholi, "Harmonic disturbance attenuation in a three-pole active magnetic bearing test rig using a modifified notch fifilter," *J. Vib. Control*, vol. 23, no. 5, pp. 770–781, Mar. 2017, doi: 10.1177/1077546315586494.

[10] S. Zheng, Q. Chen, and H. Ren, "Active balancing control of AMB-rotor systems using a phase-shift notch filter connected in parallel mode," *IEEE Trans. Ind. Electron.*, vol. 63, no. 6, pp. 3777–3785, Jun. 2016, doi: 10.1109/TIE.2016.2522948.

[11] C. Peng, M. Zhu, and K. Wang, "A two-stage synchronous vibration control for magnetically suspended rotor system in the full speed range," *IEEE Trans. Ind. Electron.*, vol. 67, no. 1, pp. 480–489, Jan. 2019, doi: 10.1109/TIE.2018.2890498.

[12] C. Peng, J. Sun, and C. Miao, "A novel cross-feedback notch filter for synchronous vibration suppression of an MSFW with significant gyroscopic effects," *IEEE Trans. Ind. Electron.*, vol. 64, no. 9, pp. 7181–7190, Apr. 2017, doi: 10.1109/TIE.2017.2694402.

[13] Y. Cai, Z. Yin, and Y. Ren, "A novel attitude angular velocity measurement method based on mass unbalance vibration suppression of magnetic bearing," *IEEE Sensors J.*, vol. 22, no. 8, pp. 7717–7726, Apr. 2022, doi: 10.1109/JSEN.2022.3157733.

[14] Y. Yang, K. Zhou, M. Cheng, and Z. B, "Phase compensation resonant controller for PWM converters," *IEEE Trans. Power Electron.*, vol. 9, no. 2, pp. 957–964, Aug. 2013, doi: 10.1109/tii.2012.2210432.

[15] P. Cui, G. Zhang, Z. Liu, and H. Xu, "Quasi-resonant control for harmonic current suppression of a magnetically suspended rotor," *IEEE Trans. Power Electron.*, vol. 34, no. 5, pp. 4937–4950, May 2019, doi: 10.1109/TPEL.2018.2865477.

[16] J. Li, G. Liu, P. Cui, S. Zheng, X. Chen, and Q. Chen, "An improved resonant controller for AMB-rotor system subject to displacement harmonic disturbance," *IEEE Trans. Power Electron.*, vol. 37, no. 5, pp. 5235–5244, May 2022, doi: 10.1109/TPEL.2021.3131756.

[17] Y. S. Ihn, J. K. Lee, and D. H. Oh, "Active correction of dynamic mass imbalance for a precise rotor," *IEEE Trans. Magn.*, vol. 45, no. 11, pp. 5088–5093, May 2009, doi: 10.1109/TMAG.2009.2029622.

[18] M. Xiang and T. Wei, "Auto balancing of high-speed rotors suspended by magnetic bearings using LMS adaptive feedforward compensation," *J. Vib. Control*, vol. 20, no. 9, pp. 1428–1436, May 2014, doi: 10.1177/1077546313479990.

[19] P. Cui, Z. Liu, and H. Xu, "Harmonic vibration force suppression of magnetically suspended rotor with frequency-domain adaptive LMS," *IEEE Sensors J.*, vol. 20, no. 3, pp. 1166–1175, Oct. 2019, doi: 10.1109/JSEN.2019.2946628.

[20] P. Cui, S. Li, and G. Zhao, "Suppression of disturbance current in active–passive magnetically suspended CMG using improved repetitive controller," *IEEE/ASME Trans. Mechatronics*, vol. 21, no. 4, pp. 2132–2141, Aug. 2016, doi: 10.1109/TMECH.2016.2555858.

[21] J. Li, G. Liu, and P. Cui, "3/2-order dual-mode fractional repetitive control for harmonic vibration suppression in magnetically suspended rotor," *IEEE Sensors J.*, vol. 20, no. 24, pp. 14713–14721, Dec. 2020, doi: 10.1109/JSEN.2020.3011927.

[22] P. Cui, Q. Wang, and G. Zhang, "Hybrid fractional repetitive control for magnetically suspended rotor systems," *IEEE Trans. Ind. Electron.*, vol. 65, no. 4, pp. 3491–3498, Apr. 2017, doi: 10.1109/TIE.2017.2752119.

[23] K. Cai, Z. Deng, and C. Peng, "Suppression of harmonic vibration in magnetically suspended centrifugal compressor using zero-phase odd-harmonic repetitive controller," *IEEE Trans. Ind. Electron.*, vol. 67, no. 9, pp. 7789–7797, Sep. 2019, doi: 10.1109/TIE.2019.2942574.

[24] Q. Chen, G. Liu, and B. Han, "Suppression of imbalance vibration inAMB-rotor systems using adaptive frequency estimator," *IEEE Trans. Ind. Electron.*, vol. 62, no. 12, pp. 7696–7705, Dec. 2015, doi: 10.1109/TIE.2015.2455022.

[25] J. Li, G. Liu, P. Cui, S. Zheng, and Q. Chen, "Synchronous vibration suppression of magnetically suspended rotor system using improved adaptive frequency estimation," *IEEE Sensors J.*, vol. 20, no. 19, pp. 11212–11220, Oct. 2020, doi: 10.1109/JSEN.2020.2997046.

[26] G. Liu, J. Li, S. Zheng, Q. Chen, and H. Liu, "Suppression ofsynchronous current using double input improved adaptive notch filter algorithm," *IEEE Trans. Ind. Electron.*, vol. 67, no. 10, pp. 8599–8607, Dec. 2019, doi: 10.1109/TIE.2019.2947852.

[27] J. Li, G. Liu, and P. Cui, "Suppression of harmonic vibration in AMB-Rotor systems using double-input adaptive frequency estimator," *IEEE Trans. Ind. Electron.*, vol. 69, no. 3, pp. 2986–2995, Mar. 2021, doi: 10.1109/TIE.2021.3065593.

[28] S. Zheng, B. Han, R. Feng, and Y. Jiang, "Vibration suppression control for AMB-supported motor driveline system using synchronous rotating frame transformation," *IEEE Trans. Ind. Electron.*, vol. 62, no. 9, pp. 5700–5708, Feb. 2015, doi: 10.1109/TIE.2015.2407857.

[29] C. Peng, K. Cai, Z. Deng, and K. Li, "Vibration torque suppression for magnetically suspended flywheel using improved synchronous rotating frame transformation," *Shock Vib.*, vol. 2019, pp. 1–13, May 2019, doi: 10.1155/2019/3607164.

[30] C. Peng and Q. Zhou, "Direct vibration force suppression for magnetically suspended motor based on synchronous rotating frame transformation," *IEEE Access*, vol. 7, pp. 37639–37649, 2019, doi: 10.1109/ACCESS.2019.2904745.

[31] L. Du, P. Cui, and X. Zhou, "Unbalance vibration control for MSCMG based on high-precision synchronous signal detection method," *IEEE Sensors J.*, vol. 21, no. 6, pp. 17917–17925, Aug. 2021, doi: 10.1109/JSEN.2021.3082695.

[32] P. Cui, L. Du, and X. Zho, "Harmonic vibration control of MSCMG based on multisynchronous rotating frame transformation," *IEEE Trans. Ind. Electron.*, vol. 69, no. 2, pp. 1717–1727, Feb. 2022, doi: 10.1109/TIE.2021.3059555.

[33] Y. Ren, X. Chen, Y. Cai, H. Zhang, C. Xin, and Q. Liu, "Attitude rate measurement and control integration using magnetically suspended control and sensitive gyroscopes," *IEEE Trans. Ind. Electron.*, vol. 65, no. 6, pp. 4921–4932, Jun. 2018, doi: 10.1109/TIE.2017.2772161.

[34] X. Chen, Y. Cai, Y. Ren, X. Yang, and C. Peng, "Spacecraft angular velocitys and angular acceleration estimation using single-gimbal magnetically suspended control moment gyros," *IEEE Trans. Ind. Electron.*, vol. 66, no. 1, pp. 440–450, Jan. 2019, doi: 10.1109/TIE.2018.2826468.

[35] X. Chen, Y. Cai, and Y. Ren, "Spacecraft vibration control based on extended modal decoupling of vernier-gimballing magnetically suspension flywheels," *IEEE Trans. Ind. Electron.*, vol. 67, no. 5, pp. 4066–4076, May 2020, doi: 10.1109/TIE.2019.2915057.

[36] Z. Yin, Y. Cai, Y. Ren, and W. Wang, "A measurement method of torque coefficient for magnetically suspended control and sensitive gyroscope," *IEEE Sensors J.*, vol. 21, no. 13, pp. 14767–14775, Jul. 2021, doi: 10.1109/JSEN.2021.3074144.

[37] Z. Yin, Y. Cai, Y. Ren, W. Wang, and X. Chen, "A high precision attitude measurement method for spacecraft based on magnetically suspended rotor tilt modulation," *IEEE Sens. J.*, vol. 20, no. 24, pp. 14882–14891, Dec. 2020, doi: 10.1109/JSEN.2020.3011066.

[38] Z. Yin, Y. Cai, Y. Ren, and W. Wang, "A precession effect suppression method for active magnetically suspended rotor," *IEEE Trans. Ind. Electron.*, vol. 69, no. 6, pp. 6130–6139, Jun. 2022, doi: 10.1109/TIE.2021.3086713.

[39] R. C. Dorf, *Modern Control Systems*, 12th ed. Reading, MA, USA: Addison-Wesley, 2011.

[40] M. Kandil, M. Dubois, and L. Bakay, "Application of second-order sliding mode concepts to active magnetic bearings," *IEEE Trans. Ind. Electron.*, vol. 65, no. 1, pp. 855–864, Jan. 2018, doi: 10.1109/TIE.2017.2721879.